UNIVERSITY OF CALIFORNIA

Los Angeles

Design and Analysis of Closed-loop Controlled Parallel-Plate Electrostatic MicroGrippers

A thesis submitted in partial satisfaction of the
requirements for the degree Master of Science
in Electrical Engineering

By

Patrick Breckow Chu

1994

The thesis of Patrick Breckow Chu is approved.

Ioannis Kanellakopoulos

William J. Kaiser

Kristofer S. J. Pister, Committee Chair

University of California, Los Angeles

1995

To my Aunt.

Contents

List of Figures

ABSTRACT OF THE THESIS

Design and Analysis of Closed-loop Control Parallel-Plate Electrostatic MicroGrippers

by

Patrick Breckow Chu

Master of Science in Electrical Engineering

University of California, Los Angeles, 1994

Professor Kristofer S. J. Pister, Chair

This work describes the design and analysis of a class of sub-millimeter scale grippers. These electrostatically-driven devices are fabricated from polysilicon using an IC-based surface micromachining process and have been designed to handle objects with dimensions in the range of 10 to 100 μm. Manipulation of substantially larger objects (up to perhaps $1mm^3$) should be possible with similarly designed grippers. The bulk of this work describes the non-linear modeling, analysis, and simulation of the electrostatic microgripper, both with and without a stabilizing feedback controller. Measurements of the open-loop system are consistent with the system model. (This thesis, along with device layout and simulation files, is available by anonymous ftp from synergy.icsl.ucla.edu.)

Chapter 1

Introduction

The electrostatic parallel-plate microgripper is an experimental design of a microgripper which may handle objects with dimensions in the range of $0.1mm$ to $1mm$ with a weight in the range of 10 to 100 μN. These gripper systems are made of polysilicon plates using a surface micromaching process and have high resolution in planar and vertical directions. Analysis and open-loop experiments show that the large area capacitive actuators for the gripper systems achieve 3 times greater displacement and nearly an order of magnitude greater force than previously demonstrated electrostatic actuators. Although these gripper structures do not yet satisfy all the specifications, fabricated test structures show that this design is realizable and the actuation concept is suitable for future microstructure designs.

In this work, the background of microgrippers and several design and fabrication considerations are presented. Analysis and stabilization of the parallel plate actuators are also discussed, where a stabilizing position feedback control law is introduced for the nonlinear system. Furthermore, computer simulation

for the closed-loop system, some static open-loop experimental results, and, finally, suggestions for future development are presented.

Chapter 2

Background

Microgrippers which can hold micron-scaled objects may be useful in many surgical and manufacturing applications. Some existing macrogrippers can handle objects with dimensions as small as $0.1mm$ but may easily damage the objects. Potentially, microstructures may achieve better performance than macrogrippers; however, existing microgrippers suffer from actuation and geometry deficiencies which limit their capabilities.

Tungsten electrostatic microtweezers were demonstrated in 1989 [1]. These tweezers are made of two long cantilever beams. The inner sides of the beams form a capacitor, allowing the tweezers to close a 3 μm gap at the tip when 150V is applied. In 1992, an "overhanging" electrostatically-driven microgripper was reported [2]. This particular microgripper, like many other electrostatically-driven polysilicon structures [3], uses interdigitated fingered capacitors to generate required forces for motions. With an initial gap of $10\mu m$, this gripper was estimated to provide $60nN$ of force at $4\mu m$ gap when 50V are applied.

Several other planar actuators based on electrostatic attraction were demonstrated to achieve greater displacement outputs than those grippers. For example, electrostatic parallelogram actuators showed $5\mu m$ of displacement with just 19V [4]. On the other hand, with an 82V applied voltage, tangential drive (T-drive) linear actuators can create a displacement of up to $32\mu m$ [5]. Due to the lack of three-dimensional resolution, the capacitor surface areas for both the gripper structures and the actuators are limited, resulting in relatively low force output and short distance of actuation. These actuation limitations are the motivations for a new actuator design.

Fabrication of a variety of three-dimensional polysilicon structures with high resolution in planar and vertical directions has been successfully demonstrated using micro-hinges [6, 7]. The design of the microgripper in this work requires the same surface micromachining process to create two large parallel plates to actuate two gripper arms. This process puts a minimal constraint on the area of these plates or length and width of the support beams. The area of the plates may range from 100 μm^2 to at least 0.1 mm^2, where the electrostatic force output increases proportionally to the increase in area. At the same time, thin and long beams ($500 \times 3 \times 1.5$ μm^3) may be used to support these large plates.

Large capacitor surface area and long and thin beams potentially allow a great range of motion because the capacitor plates initially may be set far apart from each other. However, parallel plate capacitive actuators encounter a stability problem which may limit the range of motion. The electrostatic force increases by the square of the reciprocal of the distance between the plates. On the other hand, the spring force from the support beams only increases

proportionally to the deflection of the plates. As a result, the spring force fails to balance against the electrostatic force over a large range of distances. A stabilizing controller is necessary for taking full advantage of this actuator system.

Chapter 3

Parallel-Plate Electrostatic Microgripper

The parallel-plate electrostatic microgrippers described in this work require a surface micromachining process with 2 structural polysilicon layers. Many gripper structures were fabricated at a commercial foundry called MCNC [8]. The design, fabrication, and assembly of these microgrippers are discussed in the following sections.

3.1 Design

A microgripper with a parallel-plate electrostatic actuator has a general form shown in Fig. 3.1. Two large plates are suspended by flexible beams which are connected to two stationary plates. These stationary plates are rotated off the surface of the substrate with micro-hinges and locked in place by a locking mechanism. When a voltage is applied between the two sides of the

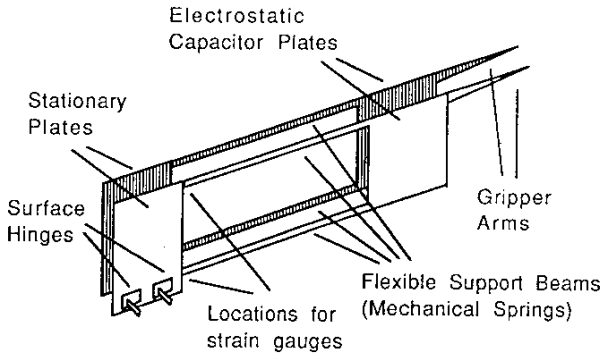

Figure 3.1: A typical parallel-plate electrostatic gripper.

plate structure, an electrostatic attractive force decreases the gap between the suspended plates, bending the flexible beams. The gripper arms need to be attached to the structure so that the displacement of the suspended plates will open or close the gripper arms. In Fig. 3.1, the gripper arms are located at one end of the gripper structure, far above the surface of the substrate. It is possible to cleave the chip in such a way that the gripper arms (and perhaps also part of the actuator) extend beyond the edge of the substrate.

Fig. 3.2 shows the layout of a similar gripper structure. In this structure, the stationary plates are anchored at opposite ends of the structure. The center rectangular plates, which are connected to the stationary plates by the thin beams, form the actuator (a variable capacitor). The T-shape structures connected to the center plates are the gripper arms. To utilize this gripper structure on a chip, one may mount the chip upside down so that the gripper arms will be extended downward.

A long thin polysilicon beam forms the electrical connection between each probe pad and the corresponding stationary plate. These beams must be designed to tolerate the torsional strain from the stationary plates when the

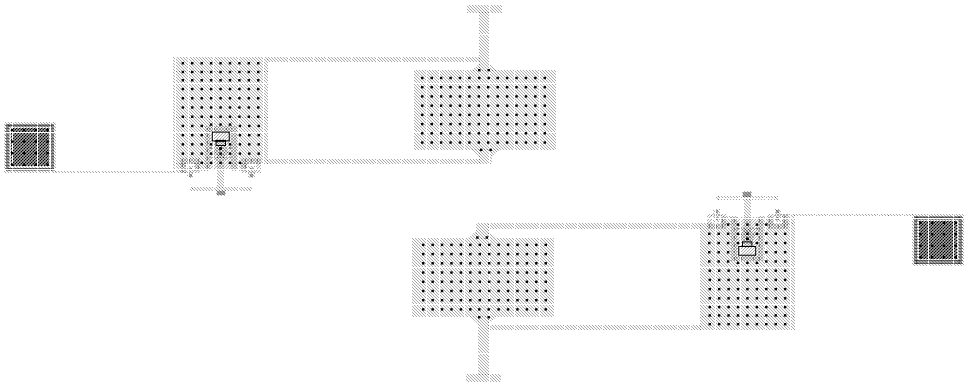

Figure 3.2: The layout diagram for a realization of the gripper design in Fig.3.1 where the stationary plates are anchored at opposite ends.

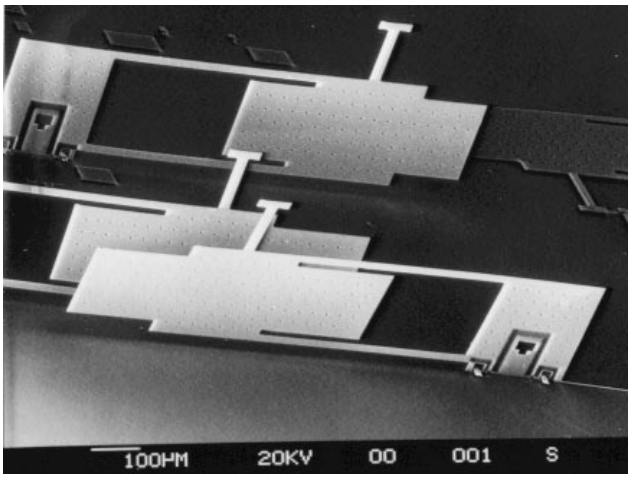

Figure 3.3: A pair of gripper-plates locked in a near vertical position by their hinges. The area of the plates is $0.09mm^2$ with $380 \times 14 \times 1.5\mu m^3$ beams and an $80\mu m$ gap at the base.

plates are rotated off the surface of the substrate. The layout diagram also shows an 80x80μm^2 probe pad on each side of test structure. These pads are used to make electrical contact to the gripper system, either with bonding wires or probes. Fig. 3.3 is a fabricated test structure with a similar layout.

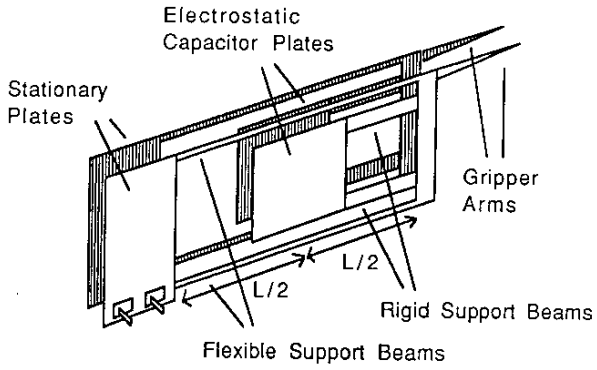

Figure 3.4: An electrostatic gripper with moment compensation, where the plates remain parallel independent of gap distance.

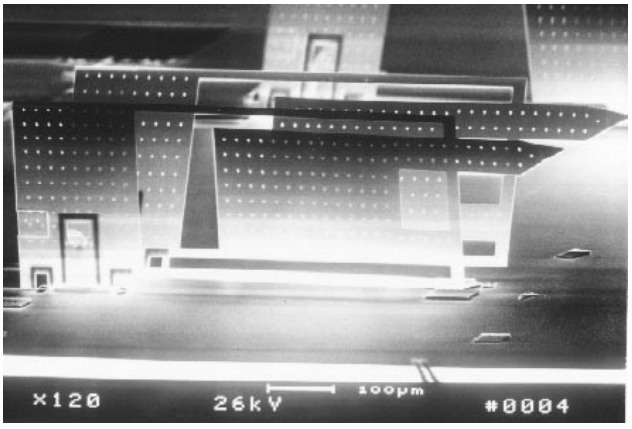

Figure 3.5: A pair of moment compensated gripper-plates. The area of the plates is $0.051mm^2$ with $500 \times 9 \times 1.5\mu m^3$ beams and an $100\mu m$ gap at the base.

Fig. 3.4 shows a realization of a parallel-plate gripper whose capacitor plates remain parallel to each other as the gap closes. The moment at the

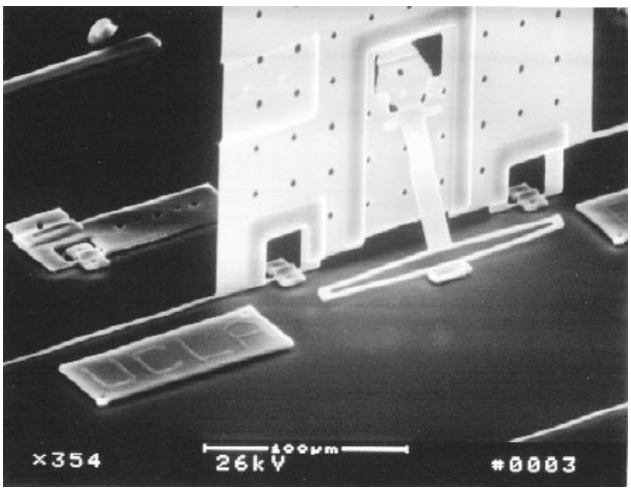

Figure 3.6: A gripper-plate locked in a vertical position by a torsional spring lock. A lever arm for assembly lies behind the plate.

center of each beam must equal zero and the moments at each end of the beam have equal magnitude but opposite sign. Unfortunately, the effective spring constant of the beams in Fig. 3.4 is 4 times greater than that in Fig. 3.1. Thus, thinner or longer beams should be used for the moment-compensated realization in Fig. 3.4. Fig. 3.5 is an example of such a structure. Although it is not necessary to require the actuating plates to remain parallel to each other, the parallel plate assumption simplifies the analysis of the system greatly.

The locking mechanism is also an important part of the gripper system. The polysilicon plates which form the gripper have a tendency to remain flat on the surface of the substrate partly due to gravity and partly due to the torsional wire connections. After these plates have been rotated upward to form the gripper, the friction in the microhinge pins occasionally prevents the plates from falling down. However, a reliable locking mechanism can prevent the gripper from falling apart after assembly. It can also guarantee that the plates stand on the substrate at the proper angle. Fig. 3.6 shows an example of

a locking mechanism which uses a spear-shaped beam connected to a torsional spring to catch the slot in the vertical plate.

3.2 Fabrication

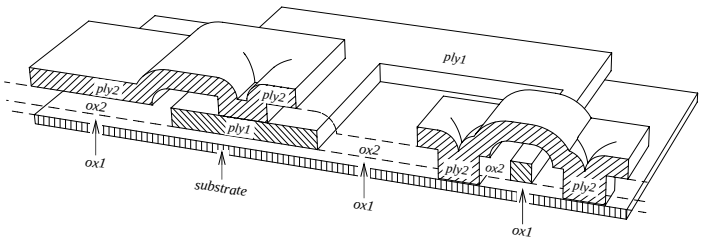

Figure 3.7: Cross section of a surface hinge. ox1 and ox2 are sacrificial layers while ply1 and ply2 are structural layers.[6]

The surface micromachining process required to build the gripper structures is based on thin film deposition with sacrificial layers. Fabrication of basic three-dimensional structures using surface hinges has been described elsewhere [6]. Fig. 3.7 shows the cross-section of a surface hinge fabricated by a three-mask process which uses polysilicon and PSG as structural and sacrificial materials respectively. In this example, ply1 and ply2 will rotate out of the plane of the substrate.

Microgrippers based on this design with different dimensions and variations have been manufactured by MCNC [8] using three polysilicon layers (only 2 may be used as structural layers), two oxide layers, one aluminum (or platinum) layer, and one nitride layer in a 7 mask process. This process has

approximately $2\mu m$ line/space resolution. Post-processing is required to release and assemble the structures on the chips from MCNC. An acetone rinse and an RIE etch may be necessary if the chips have protective photoresist on the surface. An 49% HF (or BOE) etch and DI water rinse are required to remove the PSG sacrificial layers. The assembling process may occur automatically in the HF or DI water release rinse for structure with built-in locks. Unfortunately, most of these structures had to be assembled using a probe station. Section 3.3 will discuss manual assembly in greater detail.

The MCNC surface-micromaching process does not incorporate fabrication of electronics and sensors on the same chip as the gripper structures. However, it has been demonstrated elsewhere that it is possible to integrate electronics into three dimensional structures like the microgrippers [7]. Polysilicon layers may be doped to make thin film transistors (TFT) and strain gauges. For example, it would be useful to put strain gauges at one end of the flexible beams in the gripper structures as indicated in Fig. 3.1 so that position detection becomes possible.

3.3 Assembly

Structures with built-in lock mechanism occasionally would self-assemble during the release rinses. In most occasions, manual assembly using a probe station is necessary. For structures like the gripper systems, manual assembly involves lifting plates off the surface of the substrate and rotating them until they are locked into place by some locking mechanism. The main difficulty in this process is placing a probe tip underneath a plate which is resting nearly

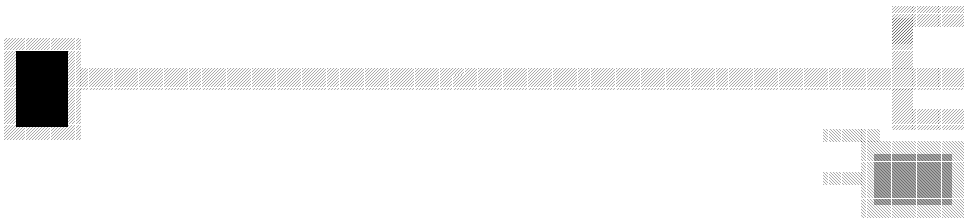

Figure 3.8: Layout of a buckled beam lever arm. The beam is $300\mu m$ long and $8\mu m$ wide.

flat on the substrate. Rotational lever arms and buckled beam jacks were designed to simplify manual assembly.

The rotational lever arm (Fig. 3.6) is made of a small rectangular plate which is free to rotate about an axis. Large plates have a greater tendency to stick to the surface of the substrate than small plates, thus it is more difficult to slide a probe tip underneath a large plate than a smaller one. As a result, the rotational lever arm may be used to lift up a large plate just enough so that a probe tip can be placed underneath the large plate. It is clear that this type of lever arm has limited benefits for assembly since one still needs to slide a probe tip underneath a thin plate on the substrate. The buckled beam jack is much more useful.

The buckled beam is composed of two parts, a long flexible beam (about 300x10x2 μm^3) with one fixed end and an anchored catch (Fig. 3.8). When the long beam is pushed from the free end, the beam will buckle upward, forming an arch. The free end may then be pushed toward the catch and lock the beam into a fixed shape. The buckled beam jack may be placed partly underneath a large plate. When the beam is arched up, the large plate rests on the top of the arch and a probe tip may easily be put underneath the plate. This jack may also be used to free large structures from potential adhesion problems.

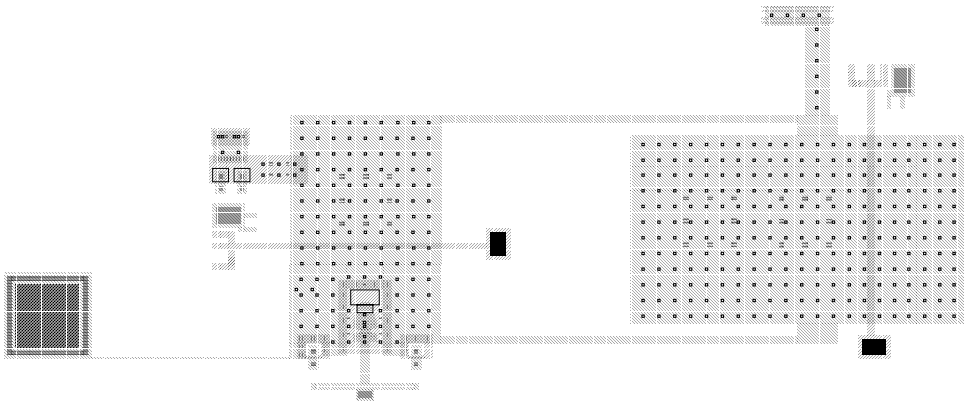

Figure 3.9: Rotational and buckled beam jacks are added to the layout of a typical gripper arm.

Fig. 3.9 shows the layout of a typical gripper arm where rotational and buckled beam jacks are added to the system to simplify assembly. One buckled beam jack is placed underneath each large plate while a rotational lever arm is placed underneath the plate on hinges. In practice, the rotational lever arm is not needed when the buckled beam jacks are present. Fig. 3.10 shows these jacks and lever arm resting on the substrate behind a rotated plate. The buckled beam jacks in this figure are locked into an arched shape.

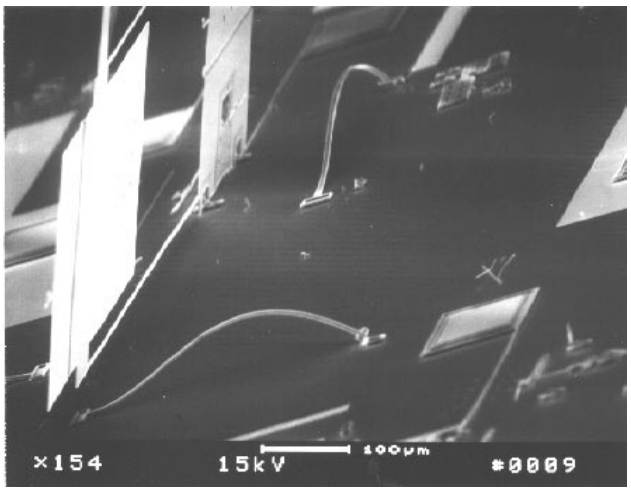

Figure 3.10: One rotational lever arm and two arched buckled beam lever arms are resting on the substrate behind a rotated plate.

Chapter 4

Analysis

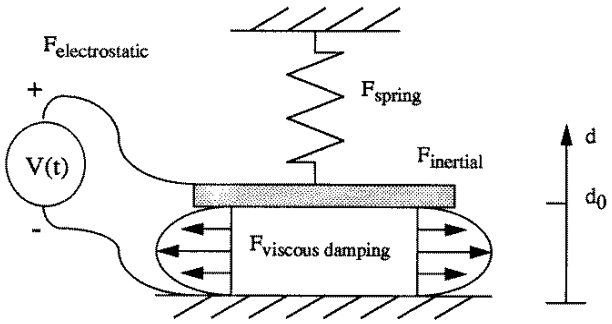

Figure 4.1: Model of a parallel-plate electrostatic actuator. Forces are positive if they tend to increase the plate separation d.

Fig. 4.1 shows a simplified model of a parallel-plate electrostatic gripper. This model is used to provide a rough approximation of the actual behavior of the gripper system. The analysis assumes that the actuator plates remain parallel as they move (as in the case for the gripper in Fig. 3.4). Furthermore, the coupling effects of the two moving masses and the four beams are ignored.

Four different forces contribute to the equilibrium and the dynamics of a

gripper system in this simplified model. The electrostatic force, f_e, due to the voltage potential V between two parallel plates with area A and a gap d is approximated by the following:

$$f_e = -\frac{1}{2}\epsilon V^2 \frac{A}{d^2} = -\frac{k_e}{d^2}V^2 \tag{4.1}$$

This force always draws the two plates toward each other.

On the other hand, the spring force, f_s, is a restoring force which tends to bring the two plates to their initial gap distance, d_0. When $d < d_0$, f_s and f_e act as opposing forces. Assume that each beam in the gripper system is a rectangular beam with length l and a cross section of height a and width b. Also assume that each spring in the system is deflected by only half the total change in gap distance from d_0. The spring force for a gripper system is then defined by

$$f_s = n\frac{3EI}{l^3}\frac{(d_0 - d)}{2} = n\frac{Ea^3b}{4l^3}\frac{(d_0 - d)}{2} = k_s(d_0 - d) \tag{4.2}$$

E is the Young's modulus of the material. n is a factor determined by the number of springs and their applications. For the system in Fig. 3.1, n is simply 4 since there are 4 springs in the system. However, for the system in Fig. 3.5, n is 16 since the effective spring constant of each spring of the moment-compensated system is 4 times greater than that of each spring in the first system.

The third force is the squeeze-film damping force, f_b, which is the only source of damping in this model of the gripper system. This force acts opposite to the direction of motion of the plates and is particularly important when the separation of the plates is very small compared to the length and width of the

plates. Starr [9] presents the expression of this damping force for a rectangular plate of dimension $2W \times 2L$ as

$$f_b = -\frac{16 c_{rect} W^3 L \mu}{d^3} \dot{d} = -\frac{k_b}{d^3} \dot{d} \tag{4.3}$$

where c_{rect} is approximately equal to

$$c_{rect} = 1 - 0.6 \frac{W}{L} \qquad 0 < \frac{W}{L} < 1 \tag{4.4}$$

The last force, f_i, is due to the inertia of the plates and is given by

$$f_i = -\rho_{PolySi} A t \ddot{d} = -m_p \ddot{d} \tag{4.5}$$

where ρ is the density of the plates with area A and thickness t. Since the sum of all forces on a system is zero, the moment compensated gripper shown in Fig. 3.4 (a 2-mass, 4-spring system) is described by the following equation:

$$2 m_p \ddot{d} + \frac{k_b}{d^3} \dot{d} - k_s (d_0 - d) + \frac{k_e}{d^2} V^2 = 0 \tag{4.6}$$

d represents the gap distance between the two parallel plates, where d_0 is the initial gap (with no voltage applied).

4.1 Static analysis of system with open-loop control

The spring-capacitor system may settle into an equilibrium position for a given voltage. At equilibrium, $\dot{d} = \ddot{d} = 0$. The force equation becomes

$$k_s (d_0 - d) = \frac{k_e V^2}{d^2} \tag{4.7}$$

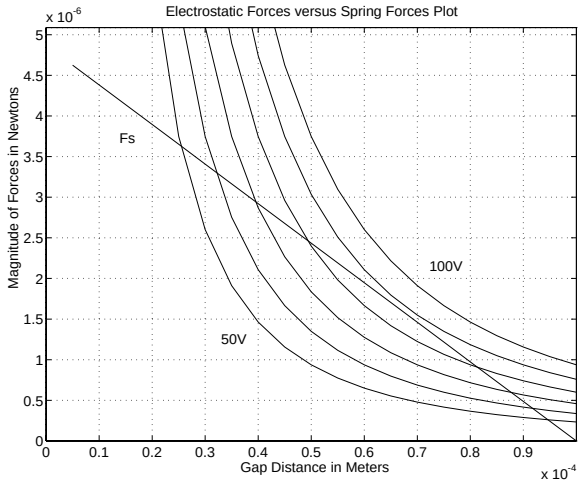

Figure 4.2: Simulated magnitude curves of F_e and F_s for the system in Fig.3.4 with $460 \times 460 \mu m^2$ plates and $500 \times 8 \times 1.5 \mu m^3$ beams. Voltages range from 50 to 100V.

This indicates that the electrostatic force and the spring force must be equal at equilibrium. At a particular applied voltage, $V_{applied}$, the equilibrium gap distance is determined by the capacitance of the parallel plate and the spring constant of the support beams.

Fig. 4.2 shows a plot of the spring force and the electrostatic force at different voltages as a function of gap distance. For a small $V_{applied}$, the spring and electrostatic force curves intersect at two points. Both intersection points are equilibrium points, at which the electrostatic force and the spring force are matched. However, only the right intersection is a stable equilibrium point. At a critical voltage, the two force curves have only one intersection point which is an unstable equilibrium. When $V_{applied}$ is above this critical voltage, the spring and electrostatic force curves have no intersection. In this case, the electrostatic force is greater than the spring force at all gap distances, thus the two plates will be pulled together until they touch. This critical voltage is

known as the pull-in voltage, V_{pi}. The corresponding gap distance is called the pull-in distance, d_{pi}. As a result, the system will be stable only when $V_{applied} \leq V_{pi}$.

Since the spring force curve is tangent to the electrostatic force curve when $V_{applied} = V_{pi}$, V_{pi} and d_{pi} may be determined by solving (4.7) and the following equation:

$$\frac{\partial}{\partial d}(k_s(d_0 - d)) = \frac{\partial}{\partial d}(\frac{k_e}{d^2}V^2) \tag{4.8}$$

It can be shown that

$$d_{pi} = \frac{2}{3}d_0 \quad and \quad V_{pi} = \sqrt{\frac{4k_s d_0^3}{27k_e}} \tag{4.9}$$

This result suggests that the actual range of operation of the spring-capacitor is only one third of its initial gap and is unaffected by the geometry of the system. However, changing the spring constant or the electrostatic constant affects the maximum value of $V_{applied}$ necessary to maintain stability.

From the force plot in Fig. 4.2, one can also estimate the force output of the microgripper. The amount of force that the actuator can output depends on the size of the object the gripper is holding. For example, suppose the gripper needs to close $20\mu m$ to come in contact with an object, about $80V$ is needed to bend the support beams to that position. Voltage higher than $80V$ will exert a gripping force onto the object. Now, assume that the object between the gripper arms will prevent the gripper plates to pull in completely, thus $V_{applied}$ may exceed V_{pi}. With $V_{applied} = 100V$, the gripper system in Fig. 4.2 can output a gripping force of $7\mu N$, $19.5\mu N$, and $89\mu N$ at gap distances of $30\mu m$, $20\mu m$, and $10\mu m$ respectively.

4.2 Dynamic analysis of system with open-loop control

Consider now the spring-capacitor system when $\dot{d}$ and $\ddot{d}$ are not necessarily equal to zero. Rearranging (4.6) yields the following:

$$\ddot{d} = -\frac{k_b}{2m_p}\frac{\dot{d}}{d^3} + \frac{k_s}{2m_p}(d_0 - d) - \frac{k_e}{2m_p}\frac{V^2}{d^2} \tag{4.10}$$

$$or \quad \ddot{d} = -K_b\frac{\dot{d}}{d^3} + K_s(d_0 - d) - K_e\frac{V^2}{d^2} =: f(\dot{d}, d, d_0, V) \tag{4.11}$$

In a vacuum (with no damping), $\omega = \sqrt{\frac{8k_s}{2m_p}}$ is the resonant frequency of the system. For the system in Fig. 4.2, $\omega \approx 6000 rad/sec$.

Consider the stability properties of the system by linearizing (4.11) about an equilibrium point using Liapunov's indirect method [10]. Arrange (4.11) into a state space form,

$$\dot{x} := \begin{bmatrix} \dot{d} \\ \ddot{d} \end{bmatrix} = \begin{bmatrix} \dot{d} \\ f(\dot{d}, d, d_0, V) \end{bmatrix} =: h(x, V) \tag{4.12}$$

Let $(\overline{x}, \overline{V})$ be an equilibrium point such that $h(\overline{x}, \overline{V}) = 0$. Then in the neighborhood of the equilibrium point,

$$h(\overline{x} + \delta x, \overline{V} + \delta V) \simeq h(\overline{x}, \overline{V}) + \left.\frac{\partial\, h(x,V)}{\partial x}\right|_{x,V=\overline{x},\overline{V}} \delta x + \left.\frac{\partial\, h(x,V)}{\partial V}\right|_{x,V=\overline{x},\overline{V}} \delta V \tag{4.13}$$

Evaluating the partial derivative shows that:

$$\delta\dot{x} = \begin{bmatrix} 0 & 1 \\ (\frac{2K_e\overline{V}^2}{\overline{d}^3} - K_s) & -\frac{K_b}{\overline{d}^3} \end{bmatrix} \delta x + \begin{bmatrix} 0 \\ -\frac{2K_e}{\overline{d}^2} \end{bmatrix} \delta V \tag{4.14}$$

The necessary condition for stability is that the real part of the eigenvalues of the system matrix must be strictly negative. As a result,

$$K_s > \frac{2K_e\bar{V}^2}{\overline{d}^3} \quad or \quad \bar{V}^2 < \frac{K_s\overline{d}^3}{2K_e} \tag{4.15}$$

From (4.11), at an equilibrium point,

$$\bar{V}^2 = \frac{K_s}{K_e}(d_0 - \overline{d})\overline{d}^2 \tag{4.16}$$

Then

$$(K_s d_0\overline{d}^3 - \frac{3}{2}K_s\overline{d}^4) < 0 \quad or \quad \overline{d} > \frac{2}{3}d_0 = d_{pi} \tag{4.17}$$

The result of this dynamic analysis confirms the earlier observation that $\overline{d}$ must be greater than $\frac{2}{3}d_0$ to maintain stability. Furthermore, all stable equilibrium points in Fig. 4.2 must lie to the right of d_{pi}.

4.3 Static analysis of system with feedback control

The spring-capacitor system is unstable mainly due to the electrostatic force increasing too rapidly compared with the spring force. It is desirable to remove the inversely proportional dependence on the gap distance square for the electrostatic force term in (4.11). Consider using the control law

$$V = \alpha u d \tag{4.18}$$

where α is a constant and u is the new control input. With this control law, the system equation from (4.11) becomes

$$\ddot{d} = -K_b\frac{\dot{d}}{d^3} + K_s(d_0 - d) - K_e\alpha^2u^2 =: f^*(\dot{d}, d, d_0, u) \tag{4.19}$$

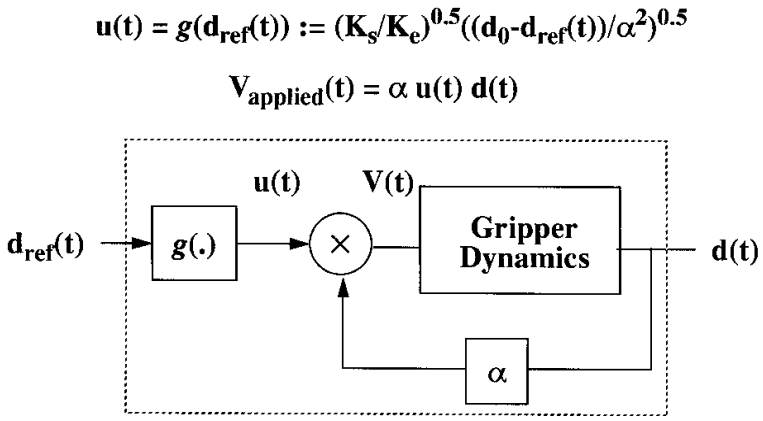

Figure 4.3: Block diagram of a nonlinear position feedback controller.

At static equilibrium where $\dot{d} = \ddot{d} = 0$,

$$K_s(d_0 - d) = K_e \alpha^2 u^2 \tag{4.20}$$

Then it can be shown that

$$\overline{d} = d_0 - \frac{K_e}{K_s}\alpha^2 \overline{u}^2 \tag{4.21}$$

$$\overline{u}^2 = \frac{K_s}{K_e}\frac{(d_0 - \overline{d})}{\alpha^2} \tag{4.22}$$

As a result, for each constant $\overline{u}^2$ input,

$$\overline{u}^2 < u_{max}^2 = \frac{K_s}{K_e}\frac{d_0}{\alpha^2} \tag{4.23}$$

there exists a unique equilibrium point $\overline{d}$. Similarly, for each equilibrium point $0 < \overline{d} \leq d_0$, there exists a unique $\overline{u}$.

Fig. 4.3 is a block-diagram representation of the proposed feedback system. In this block diagram, a reference or desired gap distance, d_{ref}, acts as the input to the closed-loop system and is used to generate u. ($\overline{d}$ and d_{ref} are equivalent.) u is then multiplied by α and d to create the actual applied

voltage $V_{applied}$. u^2 may be increased until the gap distance is near zero. In the following section, it is shown that the system model is indeed stable as d approaches zero. However, when d is near zero, the squeeze-film damping approximation may not accurately describe the real behavior of the fluid between the capacitor plates. When d is very small, the fluid may begin to act like a spring at relatively low frequencies [11].

4.4 Dynamic analysis of system with feedback control

To analyze the stability of the closed-loop feedback system with $V = \alpha u d$, we apply the same procedure from Section 4.2, (4.19) becomes

$$\dot{x} := \begin{bmatrix} \dot{d} \\ \ddot{d} \end{bmatrix} = \begin{bmatrix} \dot{d} \\ f^*(\dot{d}, d, d_0, u) \end{bmatrix} =: h^*(x, u) \tag{4.24}$$

Linearizing this equation about the neighborhood of an equilibrium point ($\overline{x}$, $\overline{u}$) yields the following:

$$\delta\dot{x} = \begin{bmatrix} 0 & 1 \\ -K_s & -\frac{K_b}{d^3} \end{bmatrix} \delta x + \begin{bmatrix} 0 \\ -2K_e\alpha^2\overline{u} \end{bmatrix} \delta u \tag{4.25}$$

The corresponding eigenvalues, λ_1 and λ_2, of the system matrix are given by

$$\{\ \lambda_1, \lambda_2\ \} = \left\{ -\frac{K_b}{\overline{d}^3} \pm \frac{1}{2}\sqrt{\left(\frac{K_b}{\overline{d}^3}\right)^2 - 4K_s} \right\} \tag{4.26}$$

This result shows that the nonlinear system is locally exponentially stable for a fixed u whenever damping is present ($K_b > 0$).

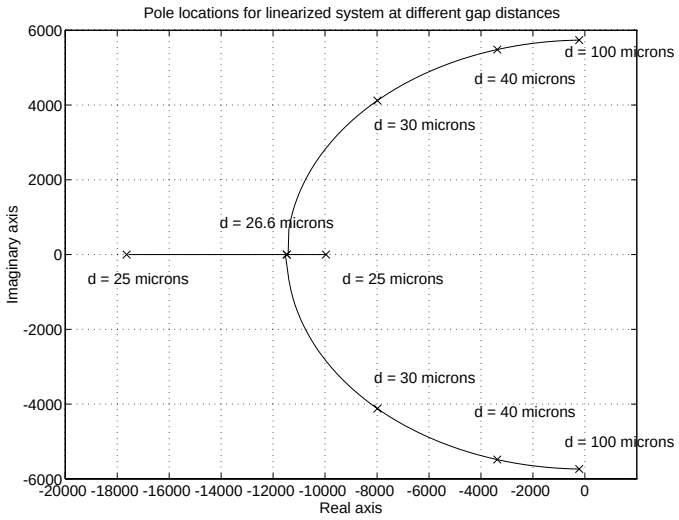

Figure 4.4: Pole locations for the linearized closed-loop system at different gap distances.

Fig. 4.4 shows how the locations of the poles change in the linearized system as the gap distance of the parallel plates decreases. The parameters used in this root locus plot correspond to the gripper system described in Fig. 4.2. In this figure, the gap distance varies from $100\mu m$ to $25\mu m$. When the gap distance is near $100\mu m$, the poles have relatively small real parts and significant imaginary parts corresponding to a large settling time and large oscillations. The damping coefficient, ζ, of the linearized system is about 0.04. As the gap distance decreases, the poles move to the left and toward the real axis due to the increasing effect from the squeeze-film damping force. Eventually, the imaginary part of the poles go to zero, indicating that the linearized system becomes overdamped ($\zeta > 1$). The system becomes critically damped ($\zeta = 1$) at a gap distance d_{crit} defined by

$$\left(\frac{K_b}{d_{crit}^3}\right)^2 = 4K_s \quad or \quad d_{crit} = \frac{(K_b)^{\frac{1}{3}}}{(4K_s)^{\frac{1}{6}}} \tag{4.27}$$

For the system in Fig. 4.4, the critical gap distance d_{crit} is $26.6\mu m$. Simulations

in the next chapter further illustrate the dynamic behavior of this gripper system.

Chapter 5

Simulation

This section presents simulation results for a closed-loop gripper system with the nonlinear controller proposed in Section 4.3. Fig. 5.1 shows plots of d_{ref}, d, $\dot{d}$, $V_{applied}$, αu of a gripper system as functions of time, where $V_{applied} = \alpha u d$. These computer results are generated using Matlab with the Runge-Kutta method and (4.19). The simulation program assumes a geometry which is the same as the moment-compensated structure in Fig. 3.4 with dimensions described in Fig. 4.2.

The system begins at $d = 100\mu m$ and $\dot{d} = \ddot{d} = u = 0$. Then the system is driven by an increasing step function in u such that the gap distance decreases by 10 micron after each step. The plot of d_{ref} shows the desired position of the gripper. Different values of u are obtained using (4.22).

The plots show the rapid increase of the damping force as the gap distance decreases. The response time to the step input also increases dramatically. Overshoots occur only when d is large, but the system clearly becomes over-damped at some distance less than $30\mu m$, correlating with the prediction in

Section. 4.4. The rise time from the first u step-input is approximately 5×10^{-4} seconds. Thus an amplifier with a bandwidth of at least 20kHz may be necessary for the controller.

The effect of the feedback control is apparent from the plot of $V_{applied}$. While d_{ref} decreases in steps, u increases in steps. On the other hand, $V_{applied}$ initially also increases with u. However, after d reaches d_{pi}, $V_{applied}$ actually decreases as d_{ref} continues to decrease so that $V_{applied}$ remains less than V_{pi} most of the time. Furthermore, the feedback controller adjusts $V_{applied}$ to compensate for oscillations in the structure such that $V_{applied}$ increases or decreases in phase with d.

Other computer simulations have also shown that the selected microgripper structure can operate at larger natural gap distances with similar performance. However, $V_{applied}$ needed to close the capacitor gaps increases significantly unless the area of the capacitor plates is increased or the spring constant of the beams is reduced appropriately.

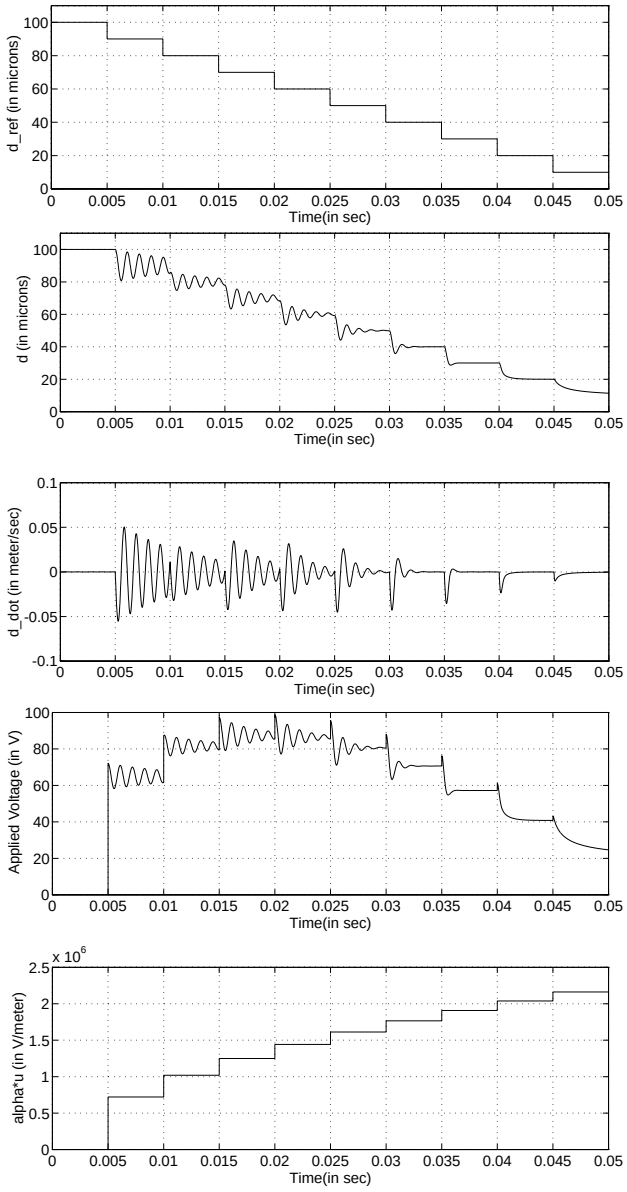

Figure 5.1: Computer simulation of the gripper described in Fig.4.2, using a second-order fixed-time-point algorithm.

Chapter 6

Preliminary Results

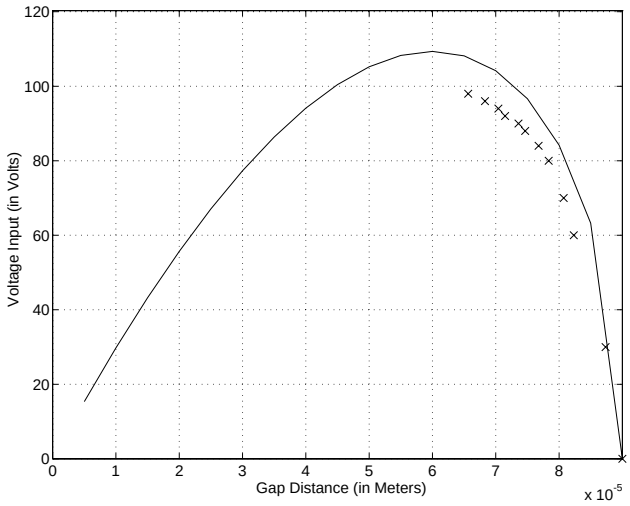

Figure 6.1: Predicted vs. observed relationship between open-loop DC voltage input and the gap distance for a gripper with $0.051mm^2$ plates and $450 \times 9 \times 1.5\mu m^3$ beams similar to Fig.3.3.

Experiments with many gripper structures were performed by applying DC voltages across the parallel-plate actuators and observing the displacement of the plates. Fig. 6.1 shows the relationship between the open-loop DC voltage input and the gap distance for a gripper with the same configuration as the

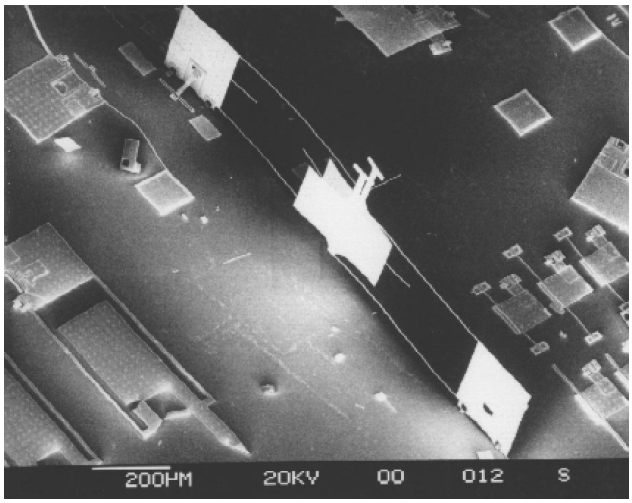

Figure 6.2: A pair of gripper arms bonded together after contact. This gripper has plates with area $0.051mm^2$ plates and $500 \times 3 \times 1.5\mu m^3$ beams with an initial gap distance of 100 μm.

gripper in Fig. 3.3. The curve represents the predicted relationship defined by (4.7). The individual points represent actual observed data before the gripper pulled in. The simulation is based on estimates for K_s and d_0 which may be different from the actual parameters from the fabricated structure. If d_0 is assumed to be 6% smaller, the fit is nearly perfect.

Another explanation for the difference between the analytical prediction and the experimental results is that the theoretical model makes assumptions about the boundary conditions of the gripper structure which are not necessarily correct. For example, the model assumes that bending only occurs in the support beams; however, bending in the stationary plates is likely to occur near the connections of the support beams. Furthermore, the torsional locks may also yield to the electrostatic force and fail to maintain the gripper plates at a constant angle during operation.

Many other structures were seen to pull in at less than the predicted voltages, possibly due to air motion and room vibrations. Grippers which touched often remained together for several seconds after the input voltage was set to zero, then returned to the open position without damage. In some cases, it has also been observed that two plates remained bonded together at the point of contact (Fig. 6.2). Oscillation has also been observed near the pull-in voltage.

Chapter 7

Conclusions

A microgripper design using parallel-plate electrostatic actuation is presented and analyzed. Theoretical analysis and computer simulations show that a position feedback control is suitable for stabilizing the capacitor-spring system. Test gripper structures not only show that the high-force-output large-motion microgripper design is realizable but also suggest that the mathematical model of the system can provide reasonable estimates of the static system. 80 to 100 μm gaps were closed with 50V to 100V.

In the future, position sensors need to be integrated into the gripper system so that closed-loop feedback testing becomes possible. One method is to put strain gauges on the support beams as described in Section 3.2. More robust controllers are necessary to improve transient behavior. More complex realizations of the gripper design must be considered to increase the gripping range. Integration of control electronics and packaging strategies for the gripper system also need to be addressed.

Bibliography

[1] N. C. MacDonald, L. Y. Chen, J. J. Yao, Z. L. Zhang, J. A. McMillan, D. C. Thomas, and K. R. Haselton, "Selective Chemical Vapor Deposition of Tungsten for Microelectromechanical Structures," *Sensors and Actuators A*, vol. 20, pp. 123–133, 1989.

[2] C. Kim, A. Pisano, and R. Muller, "Silicon-Processed Overhanging Microgripper," *Journal of Microelectromechanical Systems*, vol. 1, no. 1, pp. 31–36, 1992.

[3] W. Tang, T. Nguyen, and R. Howe, "Laterally Driven Polysilicon Resonant Microstructures," *Sensors and Actuators*, vol. 20, pp. 25–32, 1989.

[4] N. Takeshima, K. J. Gabriel, M. Ozaki, J. Takahashi, H. Horiguchi, H. Fujita, "Electrostatic Parallelogram Actuators," *Transducer '91*, pp. 63–66, San Francisco, California, June 24-27, 1991.

[5] R. A. Brennen, M. G. Lim, A. P. Pisano, and A. T. Chou, "Large Displacement Linear Actuator," *Proc. IEEE Solid State Sensor and Actuator Workshop*, pp. 135–139, Hilton Head Island, South Carolina, June 4-7, 1990.

[6] K. S. J. Pister, M. W. Judy, S. Burgett, and R. Fearing, "Microfabricated Hinges," *Sensors and Actuators A*, vol.33, pp. 249–256, 1992.

[7] K. S. J. Pister, "Hinged Polysilicon Structures with Integrated CMOS TFTs," *Proc. IEEE Solid State Sensor and Actuator Workshop*, pp. 136–139, Hilton Head Island, South Carolina, June 21-25, 1992.

[8] MCNC Center for Microelectronic Systems Technologies, Research Triangle Park, NC 27709-2889, contact: Karen Markus.

[9] J. B. Starr, "Squeeze-film Damping in Solid-state Accelerometers," *Proc. IEEE Solid State Sensor and Actuator Workshop*, pp. 44–47, Hilton Head Island, South Carolina, June 4-7, 1990.

[10] H. H. Khalil, *Nonlinear Systems*, New York: MacMillan Publishing Company, 1979.

[11] W. S. Griffin, H. H. Richardson, and S. Yamanami, "A Study of Fluid Squeeze-Film Damping," *Transactions of the ASME*, Journal of Basic Engineering, June pp. 451–456, 1966.